Investigation on Composition and Microstructural Morphology of the Fe-B-C Hardfacing Layers

M. R. Tavakoli Shoushtari*

Department of Materials Science and Engineering, Faculty of Engineering, Shahid Chamran University of Ahvaz, Iran.
Received: 12 August 2018 - Accepted: 04 January 2019

Abstract

The application of hardfacing materials for producing wear-resistant coatings on components working in wear conditions is one of the important advices in environmental protection and increasing the service life of engineering equipment. In this study, the microstructure of the hardfaced layers made by two cored wires containing Fe-B and Fe-B-C powder-based were investigated. ST37 plain carbon steel was used as the substrate and the deposition of the hardfaced layers was conducted by the flux cored arc welding (FCAW) process under single-, two-, and three-pass conditions. The microstructural and phase analyses were carried out by field emission scanning electron microscopy (FE-SEM) and X-ray diffraction (XRD), respectively. The results showed that the characteristic microstructures of the Fe-B hardfacing alloy layers comprised a matrix containing elliptical dendritic ferrite and the eutectic of (α-Fe_2B). But, the Fe-B-C hardfacing alloy layers included columnar-like Fe_2B, skeletal-like Fe_2B, daisy like $Fe_3(C, B)$ and the eutectic of (P-Fe_2B).

Keywords: Hardfacing, Microstructure, Fe-B, Fe-B-C, FCAW.

1. Introduction

Wear is one of the most important causes for the destruction and failure of the engineering components in the related industries leading to the considerable economic losses [1-3].

Producing a wear-resistant layer on the surface of the engineering components is one of the ways to control wear [4-8].

The deposition of hardfaced layer with the aim of achieving the desired thickness and metallurgical bond between the layer and the substrate can be performed by different methods of surface modification, such as arc welding [9-11], laser, plasma spray [12] and thermal spray [13]. Under impact and abrasive wear condition, the layers deposited by arc welding are preferred because it is a cost-effective method and produces relatively thicker and more resistant layers [14-17]. The ecological safety of hardfacing alloys can be assured by developing a technique of deposition of a metallic layer considering the need to save energy and resources [15]. Flux cored arc welding (FCAW), among other arc welding methods, is an economic and ecological process due to applying a high deposition rate and good efficiency. And, because of its automation ability, it can be used for coating different materials in mass scales [18]. The alloys used for depositing hardfaced layers on carbon and low-alloy steels are divided into two groups: ferrous alloys and non-ferrous alloys.

Nowadays, ferrous alloys have attracted more attention from researchers and craftsmen because of their reasonable price and a higher wear resistance compared to non-ferrous alloys [19]. Crushers and excavators work under severe wear conditions and are required to be repaired in a very short time. This is why the hardfacing of their constituents is carried out by high amounts of ferrous-based hardfacing alloys which has the least time and cost [17-19].

Fe-B-C alloy is a new wear-resistant hardfacing alloy which has drawn great consideration in recent years [20, 21]. The boron solubility in iron is very low (its maximum solubility in γ-iron and α-iron is 0.02wt% and 0.0081, respectively). Therefore, its excessive amount forms a continuous network of eutectic borides (FeB and Fe_2B) increasing the hardness and wear resistance [22, 23]. Since the specific volume and the thermal expansion coefficient of FeB and Fe_2B differ significantly, cracks are nucleated at their interface [24, 25]. Due to the presence of the weak B-B bond in the preferred direction of [002] in Fe_2B lattice, Fe_2B is considered a hard phase with intrinsic brittleness. However, regarding the fact that the boron-rich FeB phase is more brittle effect than Fe_2B, in industrial applications, there is a more tendency towards the formation of Fe_2B as a strengthening phase [26, 27]. On the other hand, the high brittleness influence of the columnar Fe_2B phase along grain boundaries leads to the surface delamination and fracture during sliding abrasive wear which in turn reduces the wear resistance [28].

*Corresponding author
Email address: m_tavakoli@scu.ac.ir

Table. 1. Welding parameters used in hardfacing process.

Process	Cored powder	Polarity	Welding velocity (mm/min)	Heat input (kJ/mm)
FCAW-Self Shielded	Ferroboron + Graphite powder	DCEP	300-330	1.62-1.92
Feeding velocity (m/min)	**Cored wire diameter (mm)**	**Arc length (mm)**	**Voltage (V)**	**Current (A)**
5-7	3.2	4-5	28-30	330-350

Therefore, in the recent years, improving the toughness of the microstructure obtained by hardfacing using Fe-B-C through controlling the Fe_2B brittleness by adding alloying elements, have been the focus of researchers [28-32].
In this study, the hardfaced layers were produced by self-shielded FCAW using two cored wires containing Fe-B and Fe-B-C alloys under single-, two-, and three-pass conditions.
The effect of C and B content on the microstructure of the hardfaced layers was investigated.

2. Materials and Methods

Six ST 37 plain carbon steel plates with dimensions of 200 × 200 × 10 mm3 were chosen as the substrate. Prior to hardfacing, top surfaces of the ST37 steel plates were cleaned with acetone to remove all surface contaminations, and then preheated to 150°C. Hardfacing was performed by self-shielded Flux-cored arc welding according to the parameters present in Table. 1.
It should be noted that welding parameters were determined under standards of ASME Section IX, parts of Qw400 & Qw216. Also, the mentioned welding process was performed as given in Table. 1. on 6 series of samples according to Table. 2. Classifying of samples was occurred on basis of cored wires and pass numbers; the three samples were welded by Fe-B cored wire and the three samples were welded by Fe-B-C cored wire during three stage process of single pass, two-pass and three-pass. Subsequently, after the prepared hardfacing coatings was air-cooled to ambient temperature, the plates were cut out to organize different test specimens.
Welded samples were labeled according to the pass numbers, respectively given in Table. 2. Fig. 1. illustrates the schematic of deposited layers on the substrate in the welding different passes along with the samples prepared for microstructural, hardness and wear studies. Chemical analysis of the base metal and hardfacing layers was obtained by spark emission spectroscopy measurement using an OXFORD INSTRUMENT machine. Moreover, according to ASTM D4951-14, boron amount was measured by Induction Coupled Plasma - atomic emission spectrometry test (ICP – AES). The plates were cut to prepare different disk-shape
specimens for wear tests, and Cubic specimens for microstructural and hardness investigations.

The cross sections of cubic specimens were mechanically finished with 2500 mesh SiC papers and finally polished with a cloth using by 1 micron diamond paste. To identify the microstructure constituents in weldment, the cross-section of the hardfacing samples was placed in etching's reagent of an aqueous solution of 10 mL HNO_3 +10mL HCl +10 mL Acetic acid.

Table. 2. Labeled samples based on welding wire and pass number.

Pass number	Cored wire	Label of sample
single pass	Fe-B	Fe-B-1
two-pass	Fe-B	Fe-B-2
three pass	Fe-B	Fe-B-3
single pass	Fe-B-C	Fe-B-C-1
two-pass	Fe-B-C	Fe-B-C-2
three pass	Fe-B-C	Fe-B-C-3

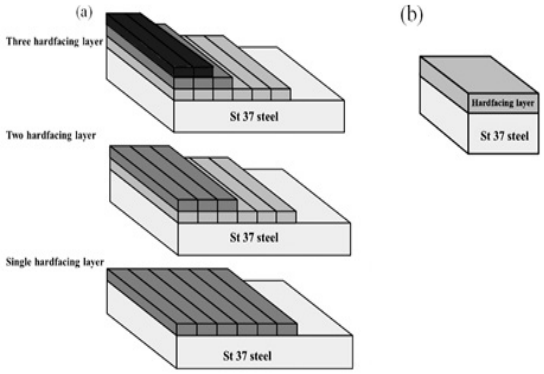

Fig. 1. Schematic illustration of (a) deposited hardfacing layers in different conditions of the welding passes, (b) sample prepared for microstructural evaluations.

Table. 3. Chemical composition of substrate and hardfacing layers (in wt. %).

Sample	C	Si	Mn	B	Fe
Base metal	0.022	0.010	0.140	-	Bal.
Fe-B-1	0.041	0.140	0.200	2.300	Bal.
Fe-B-2	0.054	0.160	0.210	2.660	Bal.
Fe-B-3	0.060	0.180	0.340	3.180	Bal.
Fe-B-C-1	0.330	0.390	0.190	2.210	Bal.
Fe-B-C-2	0.350	0.430	0.210	2.730	Bal.
Fe-B-C-3	0.380	0.500	0.250	3.120	Bal.

Microstructural examinations was studied by a TESCAN MIRA 3 Field Emission – scanning electron microscope (FE-SEM) equipped with an energy dispersive X-ray spectrometer (EDS).
For the best contrast between the different hard phases, the secondary as well as the backscattered electrons were detected. A computer-assisted Buhler Omnimet image analysis system was used to measure the morphological parameters of phases including the length and the volume fraction of particles. X-ray diffraction (XRD) of hardfacing coatings were carried out on grinded top surface of hardfaced layers using Philips X Pert-MPD system with Cu Kα radiation and 40 kV and 30 mA operating conditions and scanning angles between 20° and 90°.

3. Results and Discussion

The chemical composition of the base metal and the hardfaced layers deposited by different number of passes is given in Table. 3. Fig. 2. shows the FE-SEM micrograph of microstructures in SE contrast.
As it is evident, sample Fe-B-1 Fig. 2.(a) has led to the formation of elliptical ferritic dendrites and α-Fe_2B eutectic according to the Fe-B phase diagram Fig. 3.(a) and Fe-C phase diagram. The presence of layered ferritic dendrites can be explained according to the diagram shown in Fig. 3.(a) During the solidification process, based on the amount of boron in the alloy, the solidification line first passes through alpha (α) region and leads to the formation of pre-eutectic ferrite. As the solidification process continues and reaches the eutectic line, the melt composition changes to α-Fe_2B eutectic and the successive layers of α and Fe_2B emerge in the microstructure.

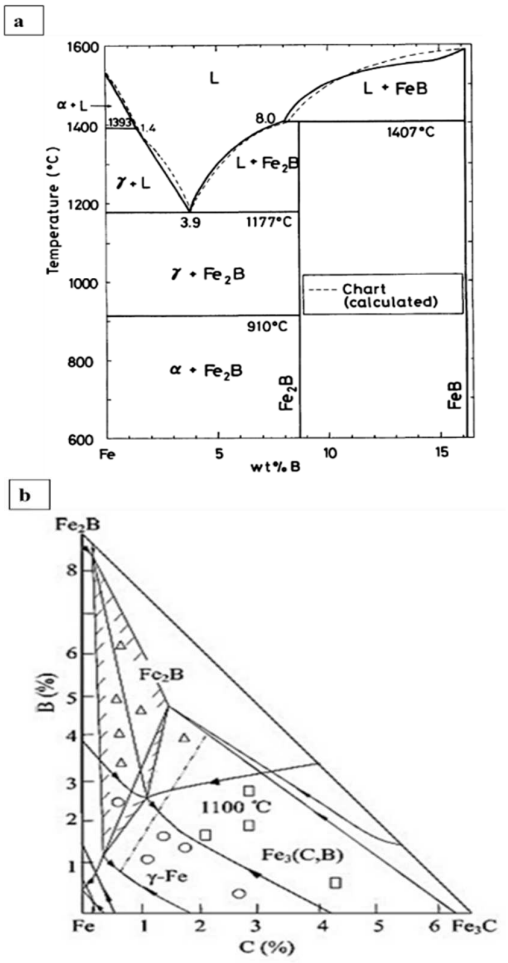

Fig. 3. (a) Fe–B phase diagram and (b) Fe-B-C phase diagram[20].

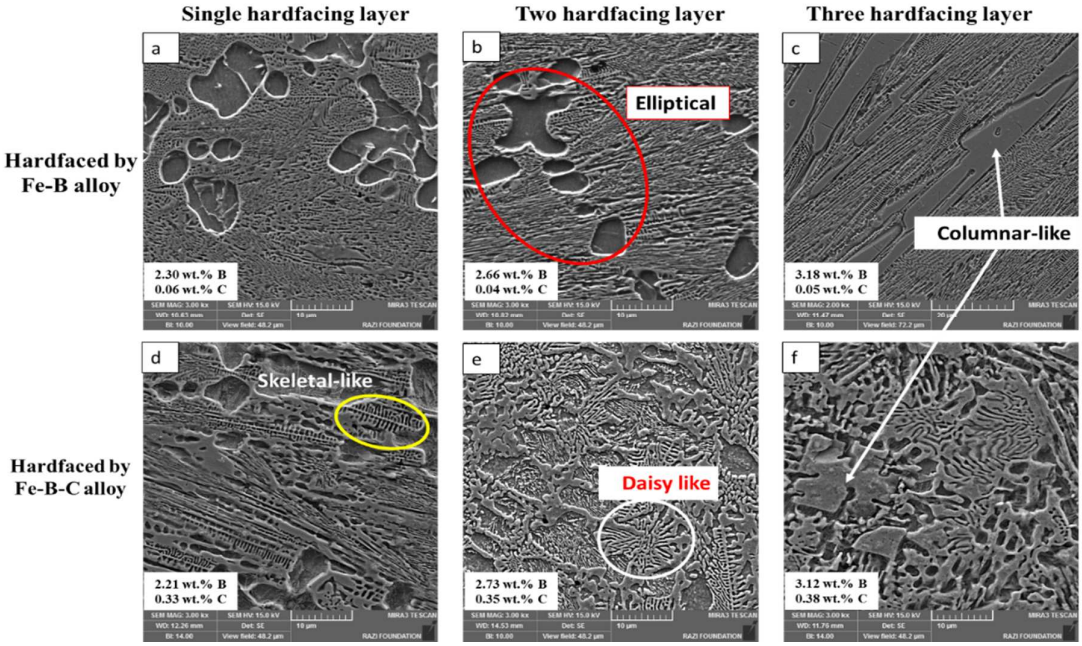

Fig. 2. FE-SEM micrograph of microstructures.

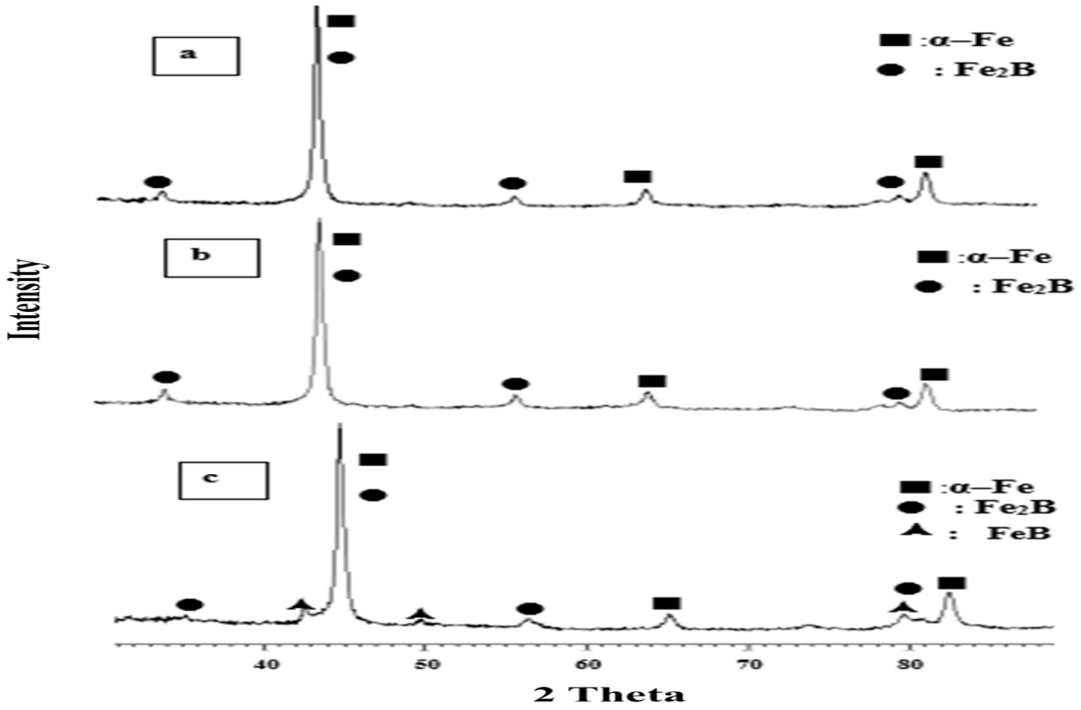

Fig. 4. X-ray diffraction pattern (XRD) from samples (a) Fe-B-1, (b) Fe-B-2 and (c) Fe-B-3.

The XRD analyses, shown in Fig. 4.(a), confirm the presence of α and Fe_2B. Fig. 5. Shows the schematic of the formation of ferritic islands and α-Fe_2B eutectic in the Fe-B-1 sample. Fig. 2.(b) shows the FE-SEM image taken from the surface of Fe-B-2. As seen, compared to the single-pass process, the two-pass deposition has led to the formation of a relatively different microstructure, consisting of ferritic dendrites, and α-Fe_2B eutectic according to the Fe-B phase diagram Fig. 3.(a) and Fe-C phase diagram Fig. 4.(b). The comparison of the images taken from Fe-B-1 and Fe-B-2 samples shows that the latter contains less layered ferritic dendrites than the former. However, in the two-pass process, as the boron content is higher, the amount of α-Fe_2B is higher (Table. 5.). Fig. 2.(c) shows the FE-SEM image taken from the surface of Fe-B-3. As seen, compared to the other two processes, the third-pass deposition has led to the formation of a relatively different microstructure containing primary columnar Fe_2B phase in between the ferritic dendrites and α-Fe_2B eutectic. The XRD analyses, shown in Fig. 4.(c), confirm the presence of α and Fe_2B. The comparison of the images taken from the two- and three-pass process shows that the latter contains less layered ferritic dendrites than the former. However, in the three-pass process, as the boron content is higher, the amount of Fe_2B is higher (Table. 5.).

Moreover, due to the non-equilibrium solidification and the presence of high boron content, at first, the primary Fe_2B is formed. As the solidification continues, α-Fe_2B eutectic is formed along with the primary Fe_2B. According to Fig. 2.(c) and XRD analysis in Fig. 4.(c), a little detrimental FeB phase and cracks have formed around Fe_2B (Table. 5.).

Fig. 6. Shows the schematic of the formation of ferritic islands and α-Fe_2B eutectic in the Fe-B-3 sample.

Table. 5. Volume fraction of each Fe-B alloy layer phase (%)

Phase	Fe-B-1	Fe-B-2	Fe-B-3
Fe	82.480	74.370	24.210
Fe_2B	17.520	25.630	68.490
FeB	-	-	7.300

Fig. 2.(d) shows the FE-SEM image taken from the surface of Fe-B-C-1. As it is evident, sample Fe-B-C-1 Fig. 2.(d) has led to the formation of elliptical pearlitic dendrites and P-Fe_2B eutectic according to the Fe-B-C phase diagram Fig. 3.(b) and Fe-C phase diagram.

The presence of layered ferritic dendrites can be explained according to the diagram shown in Fig. 3.(b) During the solidification process, based on the amount of boron and carbon in the alloy, the solidification line first passes through alpha (α) region and leads to the formation of pre-eutectic ferrite.

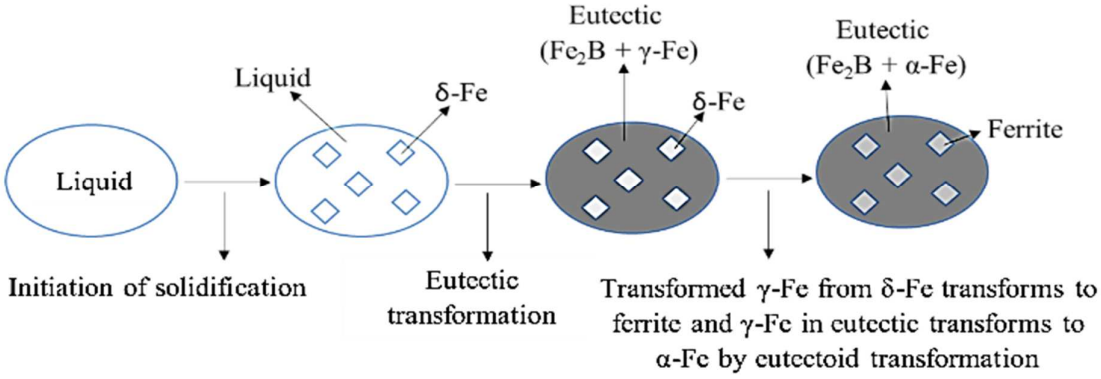

Fig. 5. Schematic of the formation of ferritic islands and α-Fe_2B eutectic in the Fe-B-1 sample.

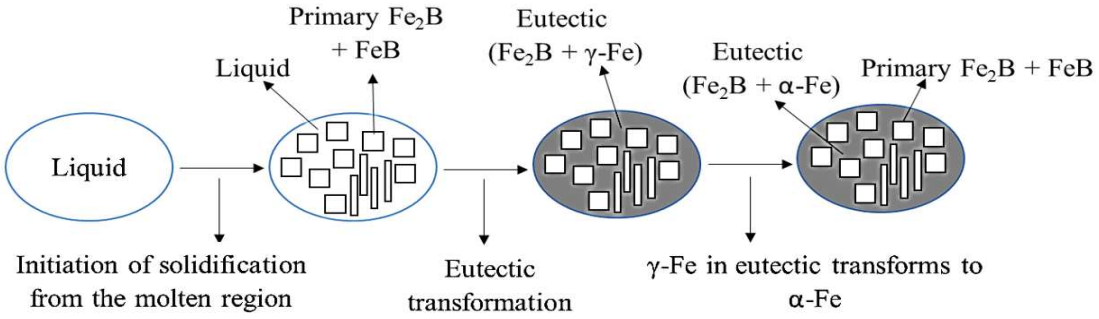

Fig. 6. Schematic illustration of the phase transformations in Fe-B-3 sample.

As the solidification process continues and reaches the eutectic line, the melt composition changes to P-Fe_2B eutectic and the successive layers of P and skeletal Fe_2B emerge in the microstructure. The XRD analyses, shown in Fig. 7.(a), confirm the presence of α and Fe_2B. Fig. 5. Shows the schematic of the formation of pearlitic islands and P-Fe_2B eutectic in the Fe-B-C-1 sample. The Fe_2B phase morphologies were rod-like and skeletal-like, as shown in Fig. 2.(d), f. The $Fe_3(C,B)$ phase morphology was daisy-like Fig. 2.(e,f). The Fe phase displayed two types of morphologies; a part of the Fe phase was present in elliptical shape, while the remaining Fe was present among daisy-like $Fe_3(C,B)$ and skeletal-like Fe_2B phases Fig. 2.(d,e).

Fig. 2.(e) shows the FE-SEM image taken from the surface of Fe-B-C-2. As seen, compared to the single-pass process, the two-pass deposition has led to the formation of a relatively different microstructure, consisting of pearlitic dendrites, and P-Fe_2B eutectic and P-Fe_3(C, B) eutectic according to the Fe-B-C phase diagram Fig. 3.(b) and Fe-C phase diagram Fig. 7.(b).

The comparison of the images taken from Fe-B-C-1 and Fe-B-C-2 samples shows that the latter contains less layered ferritic dendrites than the former. However, in the two-pass process, as the boron content is higher, the amount of α-Fe_2B is higher (Table. 6.).

Fig. 2.(f) shows the FE-SEM image taken from the surface of Fe-B-C-3. As seen, compared to the other two processes, the third-pass deposition has led to the formation of a relatively different microstructure containing primary columnar Fe_2B phase in between the ferritic dendrites and P-Fe_3(C, B) eutectic. The XRD analyses, shown in Fig. 7.(c), confirm the presence of α, Fe_2B and Fe_3(C, B). The comparison of the images taken from the two- and three-pass process shows that the latter contains less layered Fe phase dendrites than the former. However, in the three-pass process, as the boron content is higher, the amount of Fe_2B and Fe_3(C, B) is higher (Table. 6.). Moreover, due to the non-equilibrium solidification and the presence of high boron content, at first, the primary Fe_2B is formed. As the solidification continues, P-Fe_2B eutectic is formed along with the primary Fe_2B. According to Fig. 2.(f) and XRD analysis in Fig. 7.(c), a little detrimental FeB phase and cracks have formed around Fe_2B (Table. 6.).

Table. 6. Volume fraction of each Fe-B-C alloy layer phase (%).

Phase	Fe-B-1	Fe-B-2	Fe-B-3
Fe	65.94	30.62	16.19
Fe_2B	34.06	45.66	52.89
$Fe_3(C,B)$	-	23.72	28.60
FeB	-	-	2.32

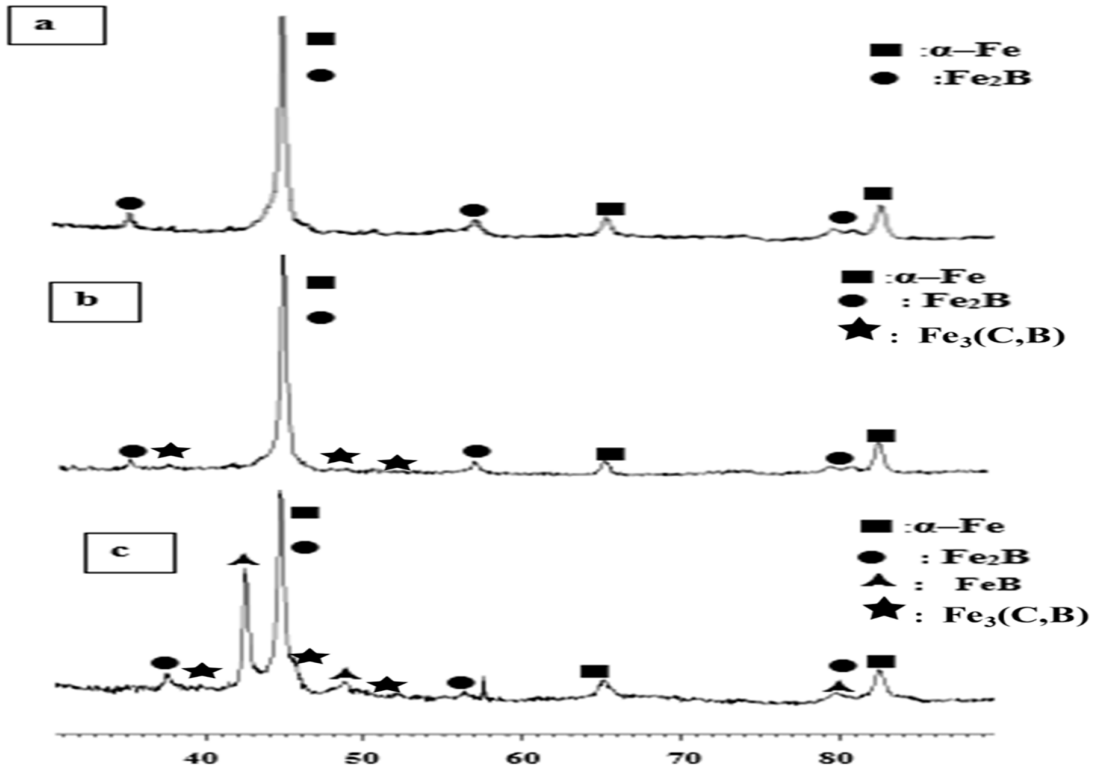

Fig. 7. X-ray diffraction pattern (XRD) from samples (a) Fe-B-C-1, (b) Fe-B-C-2 and (c) Fe-B-C-3.

SEM analysis was used to determine the microstructural distribution of the different morphologies in the hardfacing alloy layers (Fig. 3.).

The elliptical Fe phase was observed in the hardfacing alloys with a B content between 2.30 and 2.73 wt. %. Increase in the B content to 3.12 and 3.18 wt. % resulted in the formation of a new phase (columnar-like Fe_2B). As the B content increased further, the amount of elliptical Fe phase decreased and the amount of columnar-like Fe_2B phase increased (Table. 5. and Table. 6.).

Both the skeletal-like Fe_2B and daisy-like $Fe_3(C, B)$ phases existed in the hardfacing alloys where the C content ranged from 0.33 to 0.38 wt. %. Moreover, as the C content increased, the content of skeletal-like Fe_2B phase decreased, while that of daisy-like $Fe_3(C, B)$ phase increased. As a result, the volume fractions of the elliptical Fe and the columnar-like Fe_2B phases were controlled by changing the B content, while the volume fractions of the skeletal-like Fe_2B and the daisy-like $Fe_3(C, B)$ phases were synchronized by varying the C content.

4. Conclusions

The aim of this work was to study of microstructure of hardfaced layers produced by FCAW using cored wire Fe-B and Fe-B-C alloys.

The results can be summarized as follows;

1. The typical microstructures of the Fe-B alloy layers included elliptical dendritic Fe, columnar-like Fe_2B.
2. The typical microstructures of the Fe-B-C alloy layers incorporated skeletal-like Fe_2B and daisy-like $Fe_3(C, B)$ phases.
3. The volume fractions of the elliptical Fe and the columnar-like Fe_2B phases in the Fe-B alloy layers were controlled by changing the B content.
4. The volume fractions of the skeletal-like Fe_2B and the daisy-like $Fe_3(C, B)$ phases in the Fe-B-C alloy layers were coordinated by varying the C content.

References

[1] I. Kováč, R. Mikuš, J. Žarnovský, R. Drlička, J. Žitňanský and A. Výrostková, Kovove. Mater., 2014, 52, 387.

[2] J. Gou, Y. Wang, J. Sun and X. Li, J. Alloys Compd., 2017, 713, 255.

[3] J. Gou, P. Lu, Y. Wang, S. Liu and Z. Zou, Alloy. Appl. Surf. Sci., 2016, 360, 849.

[4] J. H. Kim, K. H. Ko, S. D. Noh, G. G. Kim and S. J. Kim, Alloys. Wear, (267)2009, 1415.

[5] L. Rovatti, J. N. Lemke, A. Emami, O. Stejskal and M. Vedani , J. Mater. Eng. Perform., 2015, 24, 4755.

[6] K. Gunther, J. P. Bergmann and D. Surf. Coat. Technol., 2018, 334, 420.

[7] E. O. Correa, N. G. Alcântara, L. C. Valeriano, N. D. Barbedo and R. R. Chaves, process. Surf. Coat. Technol., 2015, 276, 479.
[8] N. Yuksel and S. Sahin, Mater. Des., 2014, 58, 491.
[9] A. Gualco, H. G. Svoboda and E. S. Surian, Wear, 2016, 360-361, 14.
[10] M. H. Amushahi, F. Ashrafizadeh and M. Shamanian, processes. Surf. Coat. Technol., 2010, 204, 2723.
[11] I. Manna, J. D. Majumdar, B. R. Chandra, S. Nayak and N. B. Dahotre, Steel. Surf. Coat. Technol., 2006, 201, 434.
[12] W. Xibao, W. Xiaofeng and S. Zhongquan, Surf. Coat. Technol., 2005, 192, 257.
[13] R. Zahiri, R. Sundaramoorthy, P. Lysz and C. Subramanian, Surf. Coat. Technol., 2014, 260, 220.
[14] J. J. Coronado, H. F. Caicedo and A. L. Gomez, deposits. Tribol Int., 2009, 42, 745.
[15] V. V. Kozyrev, M. Petrov, L. G. Yu, and L. V. Kozyreva, Technologies. Weld Int., 2016, 30, 895
[16] J. N. Lemke, L. Rovatti, M. Colombo and M. Vedani, Alloys. Mater. Des., 2016, 91, 368.
[17] K. Yang, Y. Gao, K. Yang, Y. Bao and Y. Jiang, Addition. Wear, 2017, 376-377, 1091.
[18] A. Gualco, H. G. Svoboda, E. S. Surian, Weld Int., (19)2016, 255.
[19] H. Sabet, Sh. Khierandish, S. Mirdamadi and M. Goodarzi, Tribol Lett., (44)2011, 237.
[20] M. Zhuang, L. Li, J. Wang, S. Ma and S. Yuan, Microstructure and Alloys. J. Mater. Eng. Perform., (26)2017, 6182.
[21] D. Yi, J. Xing, H. Fu, Z. Zhang, J. Chen, J. Zhang, J. Peng and Y. Shi, Cast alloy. CHINA FOUNDRY, (14)2017, 145.
[22] J. Zhang, Y. Gao, J. Xing, S. Ma, D. Yi and J. Yan, Cast Alloy. Tribol Lett., (44)2011, 31.
[23] Y. Jian, Z. Huang, J. Xing and B. Wang, crystals. Mater. Charact., (110)2015, 138.
[24] L. G. Yu, X. J. Chen, K. A. Khor and G. Sundararajan, Acta Mater., (53)2005, 2361.
[25] M. Eroglu. Surf. Coat. Technol., (203)2009, 2229.
[26] Y. Jian, Z. Huang, J. Xing, B. Zheng, L. Sun,Y. Liu and Y. Liu, Tribol Int., (101)2016, 331.
[27] A. Motallebzadeh, E. Dilektasli, M. Baydogan, E. Atar and H. Cimenoglu, Evaluat. Wear., (328-329)2015, 110.
[28] Z. Huang, J. Xing and C. Guo, Addition. Mater. Des., (31)2010, 3084.
[29] D. Yi, J. Xing, Z. Zhang, H. Fu and C. Yang, Cast Alloys. Tribol. Lett., (54)2014, 107.
[30] Y. K. Singla, N. Arora and D. K. Dwivedi, A Statistical Analysis. Tribol. Int., (105)2017, 229.
[31] Y. Dawei, X. Jiandong, F. Hanguang, M. Shengqiang and L. Zhuxin, Cast Alloy. Key Eng. Mater., (457)2011, 213.
[32] Z. Huang, J. Xing and L. Lv, Cast Alloy. Mater. Charact., (75)2013, 63.